*Archaeometry* **52**, 3 (2010) 482–501 doi: 10.1111/j.1475-4754.2009.00485.x

# INVESTIGATING MATERIAL DECAY OF HISTORIC BUILDINGS USING VISUAL ANALYTICS WITH MULTI-TEMPORAL INFRARED THERMOGRAPHIC DATA*

MARIA DANESE,[1,3] URŠKA DEMŠAR,[2]† NICOLA MASINI,[1] and MARTIN CHARLTON[2]

[1]*Institute for Archaeological and Monumental Heritage (CNR-IBAM), Area di Ricerca di Potenza, C. da S. Loja, 85050 Tito Scalo (PZ), Italy*
[2]*National Centre for Geocomputation, National University of Ireland Maynooth, Maynooth, Co. Kildare, Ireland*
[3]*Urban and Territorial Systems of Engineering Laboratory, Università degli studi della Basilicata, Potenza, Italy*

*This paper shows how visual analytics methodology can be used to facilitate interpretation of multi-temporal thermographic imagery for the purpose of restoration of cultural heritage. We explore thermographic data in a visual environment from the unifying spatio-temporal perspective in an attempt to identify spatial and spatio-temporal patterns that could provide information about the structure and the level of decay of the material, and the presence of other physical phenomena in the wall. The approach is tested on a thermographic dataset captured on the façade of a Romanesque building from the 13th century—the Cathedral in Matera (Italy).*

*KEYWORDS:* VISUAL ANALYTICS, MICRO-SCALE SPATIO-TEMPORAL ANALYSIS, MULTI-TEMPORAL INFRARED THERMOGRAPHY, MATERIAL DECAY AND CHARACTERIZATION, NON-DESTRUCTIVE PASSIVE TESTING, CULTURAL HERITAGE RESTORATION

## INTRODUCTION

Infrared thermography (IRT) or thermal imaging is a technique used in various fields of application, such as to test thermal efficiency in buildings and to map building defects such as thermal bridges (Rosina and Robison 2002), to discover air leaks, moist spots and the location of electrical installations (Grinzato *et al.* 1998) and the research of hidden structure (Grinzato *et al.* 2002). During the past decade IRT has become very important in cultural heritage restoration and there are many recent works published on this topic. One of the main areas of research is the analysis of material decay in buildings of cultural or historical importance (Grinzato *et al.* 1994, 1997, 1998, 2002; Vavilov *et al.* 1997; Meola and Carlomagno 2004). IRT is used during all phases of restoration, from preliminary analysis to monitoring and management of results (Rosina and Robison 2002).

The traditional way to study multi-temporal IR images is also the simplest: we construct a profile of the temperature variations that tells us about thermal inertia. However, thermal datasets are typically very large, which means that multi-temporal and spatial patterns in the data that could tell us more about the thermal behaviour and properties of the materials are difficult to identify. In this paper we propose the use of visual analytics methodology to facilitate identification of such patterns. The proposed approach was also tested in an experimental exploration of an infrared thermographic dataset captured on a façade of a historical building.

*Received 5 December 2008; accepted 2 April 2009
†Corresponding author: email: urska.demsar@nuim.ie

The rest of the paper is structured as follows: first we present how multi-temporal IRT imaging is used in cultural heritage restoration. Then we introduce visual analytics and describe how this methodology could be used for pattern identification in multi-temporal IRT data. The following two sections present the experimental visual exploration of the multi-temporal thermal images taken of the façade of the Romanesque Cathedral in Matera (southern Italy) and the results of this exploration. Finally, we draw some conclusions and identify implications of further development of the visual exploration methodology for restoration of architectural heritage.

## INFRARED THERMOGRAPHY IN CULTURAL HERITAGE RESTORATION

IRT is a technique that allows us to measure remotely (i.e., at distance and without contact) the energy that is naturally emitted from a body in the infrared field (between 1 and 20 μm) when its temperature is greater than 0°K, that is, the absolute temperature. Theoretically, the intensity and the spectrum of that energy are functions only of the temperature of the body that emits this energy. This is the black body model that follows Stefan–Boltzmann's law, i.e.,

$$J = \sigma \cdot T^4 \tag{1}$$

where $J$ is the exitance, that is the radiation emitted per unit of surface (W/m$^2$), $\sigma$ is Stefan–Boltzmann's constant ($5.67 \times 10^{-8}$ W/m$^2$ K$^4$) and $T$ is the absolute temperature (°K). In the real world, they are also functions of surface characteristics of the material—this is the grey body (or a selective body) model. We can consequently define the infrared emissivity, which is the ratio between the emittance of the grey body and the emittance of the corresponding black body when they are at the same absolute temperature. The emittance of the grey body is measured with IRT. Through the interpretation of the radiation measured with the thermal camera it is possible to inversely determine the temperature of the body and its characteristics. However, this interpretation depends on the spectral bands, because the atmosphere does not have flat transmission properties and the emissivity itself is wavelength dependent (Maldague 2001).

There are two main forms of IRT: steady and transient. Steady thermograms give a static snapshot of the temperature measurement, while the transient methodology allows observation of a change in time of the surface temperature from a single thermogram. In addition to this, for cultural heritage restoration it is important to understand the distinction between another two types of IRT: active thermography and passive thermography. The difference between the two methods is in the source that creates the process of heat transfer. In active thermography the source is artificial, while in passive thermography it is natural.

In cultural heritage restoration we mainly use passive IRT because it is a non-destructive technique. It has been used in a number of recent cases (Rosina *et al.* 1998; Rosina and Grinzato 2001; Geraldi *et al.* 2004; Ludwig *et al.* 2004) for various purposes, for example:

- to construct, when used together with historical sources, an archaeological description of the monument and of the transformations that affected it during its existence;
- to perform a non-destructive evaluation of materials *in situ* and determine the possible presence of pathologies, conditions of deterioration and constructive techniques;
- to identify moisture in the masonry, as well as plaster and wood and the presence of extraneous materials inserted in the walls, or of masonry structure not visible to the naked eye, or of breaks in materials;
- to find relationships between decay conditions and isothermal areas;
- to use the results as a basis for a restoration plan;

• to iteratively re-evaluate and control the restoration results at every step during the restoration process.

These goals cannot be fully achieved with current methods of interpretation of IRT data, mostly because of the large number of parameters that are involved in the process of the heat transfer. The transfer depends on spectral properties of the wall (absorption, reflection and transmission), on its thermal properties (conductivity, diffusiveness, effusiveness and specific heat) and on its geometrical and material properties, such as porosity, volumetric mass and water content (Avdelidis and Moropoulou 2004). There are various examples in the literature showing how the emissivity of different materials is calculated under varying circumstances of temperature, surface condition and wavelength (Avdelidis and Moropoulou 2003). But even if the problem to determine the emissivity of materials is solved, the difficulty of interpreting the results remains, and still depends on the experience and expertise of the 'thermographer'.

To aid the interpretation of the IRT images, we suggest considering the variation of the temperature in the wall as a spatio-temporal phenomenon on a micro-spatial scale. We hypothesize that the combined spatio-temporal analysis could help the thermographer to characterize the material and its condition of decay coherently with a simplified model of the heat transfer. This task is complicated, due to the size and dimensionality of multi-temporal thermographic datasets. These datasets typically consist of a temporal sequence of thermal images (thermograms), which usually have a high spatial resolution and consequently many pixels (typically several tens of thousands of pixels per thermogram). This is probably the reason why the combined spatio-temporal analysis of multi-temporal thermographic data has not been fully investigated to date. While there are a few recent attempts to analyse multi-temporal thermographic datasets statistically, using methods such as principal component analysis (Rajic 2002; Hermosilla-Lara *et al.* 2002; Martinetti *et al.* 2004), in all these attempts the data are interpreted as images (i.e., from a spatial point of view) and separately as temporal profiles (i.e., from a temporal point of view). We instead suggest a unifying approach to data exploration using visual analytics methodology, which would enable the thermographer to look at the data from spatial and temporal perspectives simultaneously.

Our basic space in this exploration is not geographical, but covers a small area on the surface of the wall, which we term the 'micro-spatial scale'. Even though this is not a geographical phenomenon, due to the physical characteristics of the process of heat transfer in materials (which is a continuous process), the measured temperature on the surface of the wall exhibits a degree of spatial autocorrelation. It is therefore likely that the spatial and spatio-temporal patterns in the thermographic data are linked to spatial distribution of material properties, such as areas consisting of material in different stages of decay and with different types of defects.

For example, two types of patterns of interest in the thermographic data could be spatial clusters (i.e., areas of adjacent pixels with similar temperature and consequently having also the same intrinsic characteristics) and areas where there is a discontinuity in temperature values. These two patterns could point to a defect in the material, which can be either visible to the naked eye or not. Another interesting pattern could be temporal clusters—groups of (not necessarily spatially adjacent) pixels that follow a similar temperature profile throughout the sequence of thermal images. Such clusters represent thermal inertia, which measures the tendency of a substance to resist changes in temperature (Campbell 1996) and which depends on the characteristics of material composition, moisture and decay. It can be studied by looking at the temporal local variation in the temperature of a surface during a phase of cooling or warming. Because heat transfer through material is a continuous process, we can expect that most of these temporal clusters will also be spatial clusters, i.e., adjacent pixels in space will follow similar temporal

temperature profiles. Therefore we should be able to identify spatio-temporal clusters in addition to only temporal ones, as it is highly unlikely that pixels with similar temporal profiles would be randomly scattered around the study area due to the continuity in the process of heat transfer through material.

There are many ways to find clusters and similarities in data. However, in large and multi-dimensional spatial datasets, which thermographic data typically are, this is not always easy or computationally feasible. To facilitate this process we suggest exploring the data visually using visual analytics methodology, which we introduce in the next section.

## VISUAL ANALYTICS OF MULTI-TEMPORAL INFRARED THERMOGRAPHIC IMAGERY

Ever-increasing amounts of spatio-temporal data often present a problem for scientists in various disciplines who are trying to make sense of the data. Visual spatial data analysis as a part of exploratory spatial data analysis employs visual exploration of these large datasets to identify spatio-temporal and other patterns that subsequently serve as a basis for hypothesis generation and analytical reasoning about the data and the phenomenon that generated these data. Such a multidisciplinary data explorational approach, where visualization serves as a tool for provoking ideas and thoughts, is the research subject of visual analytics [National Visualization and Analytics Center (NVAC) 2005], a recent new sub-discipline of information visualization. Visual analytics and, in the case of spatial data, geovisual analytics (Andrienko *et al.* 2007) are concerned with analytical reasoning about the data through visual exploration. Its methods are used to identify patterns and thereby derive knowledge from large, highly dimensional spatial and spatio-temporal datasets. Using this methodology for the spatio-temporal analysis of multi-temporal IR thermographic data could therefore facilitate interpretation of the images and help with the characterization of the type of material and the stage of material decay.

To test this hypothesis, we decided to perform a visual analytical exploration of multi-temporal IRT images of the façade of a historic building in an attempt to see if we can identify patterns of similarities and differences in the spatio-temporal temperature variation in the wall, and if such patterns could be linked to the type of material and level of decay. For this experiment we re-used a visual exploratory environment first built for environmental analysis (Demšar 2007) and subsequently used in methodological work on combining spatial statistics with geovisualization (Demšar *et al.* 2008a,b). The environment was built using GeoVISTA Studio (Gahegan *et al.* 2002) and consisted of a self-organizing map (SOM), a temporal parallel coordinates plot (PCP), a parallel coordinates plot linked to the SOM (SOM PCP) and a map, also linked to the SOM. The rest of this section briefly describes each of these visualizations and then presents the physical reasoning behind the approach, i.e., why we think these methods are appropriate for analysis of multi-temporal IRT imagery.

A SOM is a neural network which maps a multidimensional space on to two dimensions while preserving the topology and the probability density of the input space (Kohonen 1997). This means that the similarity patterns that exist in the input space are preserved in the two-dimensional (2D) output space. Because of this property, a SOM is a popular method for knowledge discovery from spatial and spatio-temporal data and has been used for this purpose in a number of recent cases (Koua and Kraak 2004; Guo *et al.* 2005; Skupin and Hagelman 2005; Demšar 2007, to list a few). The output space of the SOM is usually represented either as a regular grid or as a hexagonal lattice. The most common visualization of the SOM result is a U-matrix, where graphic properties of each lattice cell depend on the similarity measure of the elements that were assigned to that cell (Vesanto 1999). The GeoVISTA Studio SOM (Guo *et al.*

2005), which we used in our exploratory environment, is implemented as such a hexagonal lattice and consists of two types of cells: node cells which represent the nodes of the SOM, and distance cells which are dispersed among the node cells and show the level of similarity between neighbouring node cells. This level is indicated by the grey shade of each cell: the darker the cell, the more dissimilar it is from the cells in its neighbourhood. This effectively means that groups of lighter cells in the lattice indicate clusters and groups of darker cells the borders between clusters. In this particular SOM implementation we can also see the distribution of the data in the cells: this is shown through the size of the circles that are drawn over the node cells. The larger the circle, the more data elements the SOM mapping assigned to the node cell of that particular circle. The circles are coloured by draping a smooth 2D colour map over the lattice and their colour is subsequently transferred into all other visualizations for clearer identification of the clusters elsewhere. More details about this SOM implementation are given in Guo *et al.* (2005).

For this experiment we used two parallel coordinates plots (PCPs), a temporal one and one linked to the SOM (Guo 2003; Guo *et al.* 2005). At first sight this might imply redundancy, but the reason behind this is that each of these PCPs is suitable for identification of a different type of pattern. The temporal PCP was used for identification of temporal trends. While the SOM PCP distorts the statistical distribution of data through nested-means scaling and thereby makes identification of temporal trends difficult; it was originally developed for cluster analysis, which cannot be performed in the temporal PCP in the same easy way, but which we considered necessary for identification of temporal clusters in temperature behaviour. We therefore decided to use both versions of the PCP in our environment. In the temporal PCP each data element is represented as a polygonal line which intersects each of the axes (dimensions) at the value that particular data element has in that particular dimension (Inselberg 2002). Each axis of this PCP is linearly scaled from the minimum value across all dimensions to the maximum value across all dimensions—this version of a PCP facilitates identification of temporal trends (Edsall 2003). In contrast, each polygonal line in the SOM PCP corresponds to one node cell from the SOM and its width corresponds to the size of the circle that belongs to that same node cell in the SOM (Guo 2003). This property is useful for cluster analysis and interactive selection of subsets of clusters. The colour of the polygonal lines in both PCPs is inherited from the SOM, which helps with the identification of the similarities in temporal trends in the data.

A spatial visualization, the geoMap, is used as a thematic map showing the spatial distribution of the SOM clustering. The SOM clustering that we calculated is inherently non-spatial, as the algorithm used is the original Kohonen SOM. This version of the SOM algorithm is based on non-spatial attribute values in contrast with, for example, the GeoSOM (Bação *et al.* 2005), where the spatial position is one of the clustering attributes. The spatial distribution of the SOM clusters is shown through the colours on the map, which are inherited from the SOM via visual brushing (Gahegan *et al.* 2002; Guo *et al.* 2005).

Using the described visual analytical system we explored thermograms in an attempt to identify spatial and spatio-temporal patterns in the data. We believe that such patterns can potentially provide information about the structure of the wall and the presence of physical phenomena in the wall, as explained in the rest of this section.

In order to be able to interpret the visually discovered patterns, we first need to consider what our data consist of. We have a series of static steady thermograms (i.e., thermograms that measure surface temperature at one particular point in time), which all cover the same area, have the same spatial extent and the same spatial resolution, but which were taken at different points in time. These thermograms can be connected through location into a spatio-temporal dataset, using spatial overlay. This means that a particular pixel in one thermogram can be linked to the same

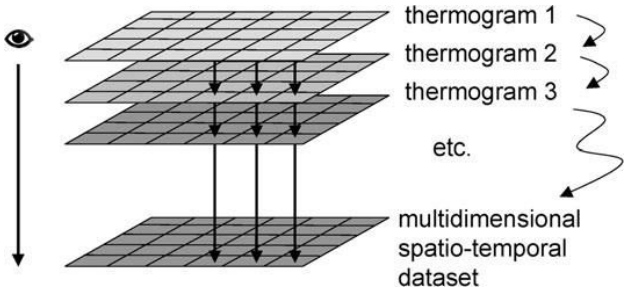


Figure 1 *Construction of the spatio-temporal dataset from thermograms using spatial the overlay principle. Data consist of pixels, which have identical spatial extent and spatial location in all thermograms. Pixels in different thermograms can therefore be connected to each other with spatial overlay, as if looking through each pixel in the stacked thermograms from top down and collecting temperature measurements for one particular pixel from each thermogram as dimensions (attributes) of the dataset.*

pixel in all other thermograms, which is possible because of the same spatial extent and resolution of all thermograms. Data objects in our dataset are therefore pixels. Dimensions (attributes) in the dataset are separate temporal measurements of temperature at each pixel. Construction of the dataset is shown schematically in Figure 1.

Physically, pixels in our dataset represent small square areas on the wall (in our case of the 4.62 mm spatial resolution, as explained later in the paper). Therefore, to be able to interpret discovered patterns from the physical point of view, we need to consider the energy conservation applied to a very small volume of opaque material. In the absence of an internal energy source, this becomes:

$$\frac{\partial T}{\partial t} = \alpha\left(\frac{\partial^2 T}{\partial x^2} + \frac{\partial^2 T}{\partial y^2}\right) \tag{2}$$

where $T$ is the temperature, $t$ is the interval of time and $\alpha$ a factor which depends on the properties of the material (thermal conductivity, density and specific heat capacity). For each pixel the spatial gradient of temperature (represented in each line of the temporal PCP) can be considered constant, so the temporal gradient will depend only on $\alpha$. Consequently pixels from areas of material with similar characteristics (and therefore with same value for $\alpha$) are represented in the temporal PCP by lines that follow similar trends, which represent localized temperature profiles (i.e., a temperature profile for each pixel).

The SOM groups pixels with similar temporal temperature profiles into clusters that are visible in the SOM and in the SOM PCP. In addition to this, the colours from the SOM are transferred to all other visualizations as described earlier, so that clusters of similar temporal temperature behaviour (i.e., temporal-thermal clusters) can also be investigated in other visualizations. These clusters are shown in other visualizations as groups of graphic entities with the same or similar colours. These entities represent data elements and vary from visualization to visualization (e.g., grid cells in the geoMap or lines in the temporal PCP). In particular, spatial distribution of the SOM clusters can be observed in the geoMap—looking at groups of similarly coloured pixels in the map can tell us if these temporal–thermal clusters have any particular spatial pattern or if they are distributed randomly over the entire exploration area. The combination of SOM and the geoMap therefore provides a qualitative visual way to observe similarity in the variation of temperatures over space and time simultaneously.

As is usually the case with visual data exploration, any discovered patterns need to be validated to separate spurious patterns from real patterns. Results should therefore be validated from a

macroscopic and qualitative point of view, only then can they be used as a basis for conservation interventions. We have attempted to perform this validation for the results of our experiment by comparing the results against background information about the material and structure of the wall. A more in-depth validation, however, was beyond the scope of this paper, which focuses on the application and feasibility of a new data analysis method, i.e., the visual analytical exploration of thermograpic data.

## CASE STUDY: THE FAÇADE OF THE CATHEDRAL IN MATERA, ITALY

The Cathedral of Matera is one of the most remarkable churches of the Romanesque style in southern Italy. It is located on a panoramic spur facing the famous ancient town 'The Sassi' of Matera, and is included in the UNESCO World Heritage list. The church has a Latin cross plan, composed of three longitudinal aisles cut transversally by a transept. It was built between 1230 and 1270, on two pre-existing crypts and the foundations of a church dedicated to St Eustachio. Since 1389 it has been dedicated to Santa Maria della Bruna. The external structure, constructed of calcarenite ashlars (stone blocks), preserves its original Romanesque characteristics, but the interior of the church has been modified by successive changes—for example, the central nave is mostly 17th century.

Currently the Cathedral is under restoration. The works are mainly aimed at the structural rehabilitation of pillars, columns and roofing, as well as restoration of the main façade facing west. The calcarenite masonry of this façade has been the object of a multi-temporal thermographic analysis at the Institute for Archaeological and Monumental Heritage (CNR-IBAM) in Potenza. The main reason for choosing this façade as the subject area for our experiment is that it is built of only one building material, i.e., the locally quarried calcarenites. The presence of only one building material simplifies evaluation of the exploration results obtained with visual analytics, which was important as we intended to see if visual analytics is useful for identification of degradation pathologies of one material. Choosing a façade or a wall consisting of several materials would complicate this evaluation.

The calcarenites of the façade originated in a Plio-Pleistocene formation (Calcarenite di Gravina) overlapping the Mesozoic–Cenozoic limestone successions of the Apulian foreland. These calcarenites are soft and porous and suffer from deterioration as a result of weathering. In particular, they are affected by alveolization, which is the effect of deterioration mechanisms induced by water imbibition and/or salt crystallization (Andriani and Walsh 2007). In our experiment we attempted to identify the type of extent of typical degradation pathologies of calcarenite (i.e., alveolization).

For our experiment, the thermographic data were collected picturing an area on the main façade of the church, size 1.28 × 0.95 m and located to the right of the main entrance to the cathedral (Fig. 2). The area consists of calcarenite ashlars affected by different types of decay, such as alveolization, loss of material, differential erosion, alteration in colour and formation of crusts. These decay types are described here from the macroscopic point of view and can be seen in Fig. 2, where we have numbered the ashlars.

The most prevalent type of decay in the wall is alveolization or cavernous decay, i.e., the presence of alveoli (small cavities or pits) on the surface of the wall. Alveoli are present in all ashlars (Fig. 2), even though their dimensions and their distribution changes throughout the wall surface. Additionally, in some areas of the wall we have a presence of other categories of decay on top of alveolization. The surface of some ashlars (1, 2, 3, 4, 5 and 9) is in good condition of conservation and is still relatively smooth, even if there are a few shallow hollows present here and

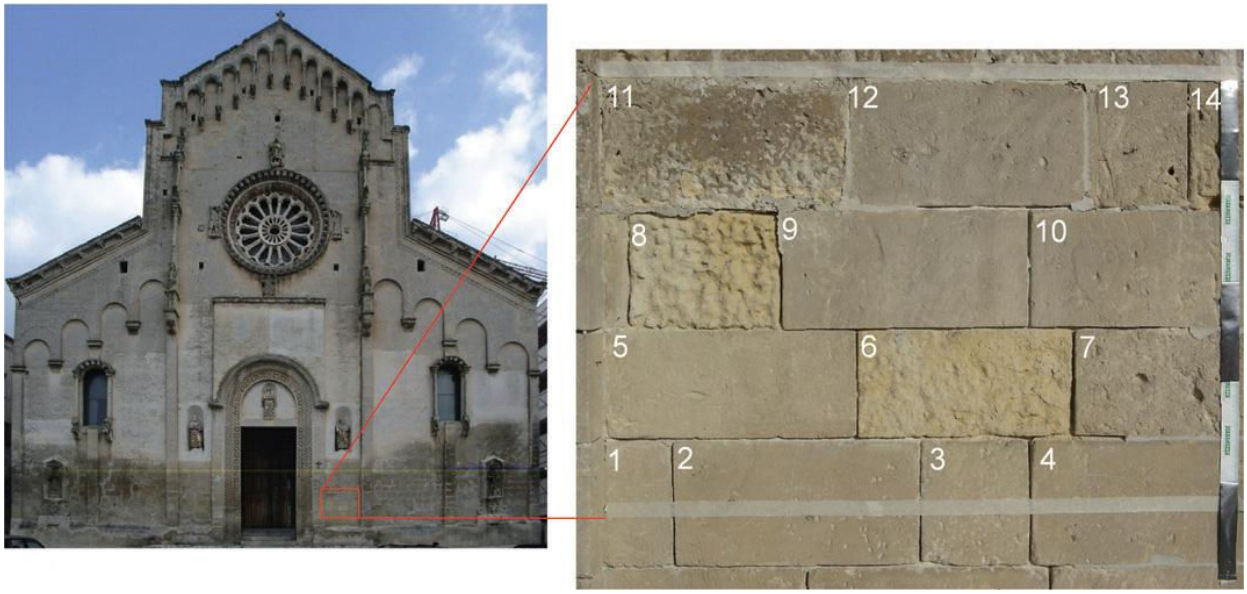


Figure 2 *The main façade of the Cathedral in Matera and the location of the thermographic data collection. In the insert on the right, the ashlars (stone blocks) are enumerated for easier comparison in the subsequent visual analysis.*

there. Other ashlars (10 and 12) are lightly weathered—the condition which is characterized by eroded surface and isolated alveoli of different sizes (from the order of millimetres to centimetres) and depths. Significant alveolization is present in ashlars 7, 13 and 14; this state is characterized by larger (in the order of centimetres) and deeper alveoli that are beginning to be connected. In these three ashlars there is also a significant loss of material in areas which are differentially eroded. Their surface also exhibits a change in colour, which is clearer to see in ashlar 7 and more yellow in ashlars 13 and 14, probably due to crystallization of soluble salts. Three ashlars (6, 8 and 11) exhibit a high level of alveolization, which is characterized by an irregular surface of large alveoli of irregular depth and serpentine shape. Additionally, ashlar 11 is of a darker colour due to the presence of a crust, probably a remainder of a past protective treatment.

The gaps between adjacent calcarenite ashlars are filled with mortar (Fig. 2), used during a past restoration. The mortar is, in some places, partly detached and in other places completely missing, leaving empty spaces between the ashlars.

These characteristics of the wall can help us define what patterns we would ideally like to discover with the visual analytical exploration of the thermographic data in our experiment, i.e., patterns that characterize:

(1) calcarenite surface with a few shallow alveoli (ashlars 1, 2, 3, 4, 5 and 9);
(2) light alveolization (isolated and slightly deeper alveoli) and diffuse erosion of the surface (ashlars 10 and 12);
(3) significant alveolization (alveoli deeper than those of pattern 2) that starts to be connected (ashlars 7, 13 and14);
(4) strong alveolization and irregular surface (ashlars 6, 8 and part of ashlar 11);
(5) dark = coloured crust probably attributable to a past protective treatment (ashlar 11);
(6) the behaviour of the mortar between ashlars;
(7) other phenomena that are not recognizable in the photo taken in visible light, such as the presence of humidity in the wall.

In the following experiment we use this list as a basis for interpretation of patterns, which were discovered during our visual exploration.

## THE EXPERIMENT: ACQUISITION OF INFRARED THERMAL IMAGES AND PRE-PROCESSING OF THE DATA

The thermal camera used for the experiment was an AVIO TVS 600 microbolometric. It works in the long-wave spectrum, between 8 and 14 μm, has a lens of 35 mm and a target range of 3.30 m, measured from the focus to the wall. The spatial resolution (i.e., the size of the image pixel) is 1.4 mrad.

The acquired thermograms were exported for our experiment as images with pixel size (spatial resolution) of 4.62 mm. Spatial resolution is a very important factor in IRT analysis, because the correct evaluation of the temperature depends on it. In our case study it is important that the pixel size is small enough to detect the signs of the alveolization which depend on the type of investigated material. The alveoli on the surface of the calcarenite can have different shapes and dimensions and a non-uniform distribution. Therefore, a high spatial resolution of the measurements can be very important to discriminate between calcarenite in a good conservation state from calcarenite with a higher level of deterioration.

We captured thermal images during an evening time period of 3 hours in the month of July, when the wall was cooling off after being exposed to the afternoon sun. The time of the year and the short time range of measurement acquisition allow us to consider wind speed and humidity as almost constant. The thermal images were taken when it was already dark, so that no new external heat was added to the wall by the sun during the data capture period. A thermal image was recorded every 30 min, from 21.00 to 00.00 hours. There were seven sampling times in total, which correspond to temporal dimensions of the dataset. The external air temperature during the capture period decreased from 27°C at 21.00 to 25°C at 22.00 and was then relatively constant within 1/10 of a degree until 00.00 hours. Each of the seven thermal images was of the same size (320 × 236 pixels, i.e., 75 520 pixels in total) and the value of each pixel represented the temperature of the corresponding area on the wall. Table 1 presents an overview of the temperature range, external air temperature and times of data capture.

The images were combined into a seven-dimensional dataset, with pixels as basic data elements and seven temporal temperature measurements as seven attributes (dimensions). We explored this dataset in the previously introduced visual exploration environment. After the initial exploration we added a further seven attributes, which were calculated as the difference between the temperature of each pixel and the external air temperature at a particular moment in time, as

Table 1 *Times of data capture, external air temperature and the range of min.–max. measured temperature in each thermal image*

| *Attribute ID* | *Time of capture* | *External temperature* (°C) | *Min. measured temperature* (°C) | *Max. measured temperature* (°C) |
|---|---|---|---|---|
| P70 | 21.00 | 26.900000 | 22.790000 | 33.290000 |
| P71 | 21.30 | 26.300000 | 22.990000 | 33.470001 |
| P72 | 22.00 | 25.400000 | 22.879999 | 33.380001 |
| P73 | 22.30 | 24.900000 | 25.879999 | 34.320000 |
| P74 | 23.00 | 25.000000 | 22.920000 | 32.500000 |
| P75 | 23.30 | 24.900000 | 18.469999 | 31.950001 |
| P76 | 00.00 | 25.000000 | 25.840000 | 33.369999 |

described below. This was done to see if it was possible to identify certain patterns which we could not see in the exploration of only temperature measurements.

## RESULTS: VISUAL EXPLORATION OF THE THERMOGRAPHIC DATA

For the initial visual exploration we first calculated the SOM clustering based on the seven temperature values measured for each pixel (attributes P70, P71, . . . , P76, as in Table 1). The results of the clustering were transferred to other visualizations, i.e., the map, the temporal PCP and the SOM PCP, by visual linking through colour, as described in previous sections. Figure 3 shows the visualizations at this stage in the exploration. The map (Fig. 3 (a)) shows a grid of pixels that corresponds to the thermal images. The SOM (Fig. 3 (b)) and the SOM PCP (Fig. 3 (d)) show the result of the clustering. The temporal PCP (Fig. 3 (c)) and the SOM PCP have axes, each of which corresponds to one temporal temperature measurement: P70 at 21.00, P71 at 21.30, . . . P76 at 00.00 hours (Table 1). While in the temporal PCPs all axes are identically scaled, from the minimum to maximum temperature across all axes (i.e., from 18.47 to 34.32°C), the SOM PCP has a non-interactive fixed nested-means scaling for each axis. The lines in the SOM PCP represent the clusters from the SOM (circles) and the lines in the temporal PCP represent the grid cells from the map. The colour of the clusters is transferred to all other visualizations, meaning that the pixels in the map and the lines in the SOM and the PCP are assigned the colour according to their position in the SOM.

While we only used temporal information as the input to the SOM, there is a large amount of spatial clustering present, which can be seen by looking at the colour of neighbouring pixels in the map (Fig. 3 (a)). The colour of these pixels comes from the SOM (Fig. 3 (b)) and the fact that the map shows a structured picture rather than just a random scattered pattern means that there is spatial autocorrelation of the temporal trends present in the temperature measurements that the SOM identified. The SOM shows one large cluster (the large blue circle in the bottom-left corner) and a more or less equal distribution of other data elements into other areas of the SOM (all of the circles except the large blue one are of approximately the same size).

Looking at the map, the temporal PCP (Fig. 3 (c)) and the SOM PCP (Fig. 3 (d)) we can see that the majority of the pixels in the map (blue areas) follow a similar temporal trend (see the corresponding blue lines in both PCPs), with relatively low temperatures throughout the entire time period. These pixels are all grouped in the dark blue cluster, which is the largest cluster in the SOM as mentioned above. The track of this cluster in the SOM PCP (Fig. 3 (d)) is distinctively separated from all other values. Examining the box plots on each axis and at the values of the blue cluster in the temporal PCP (Fig. 3 (c)) we see that the blue values are below average at all times, i.e., these are the coolest areas of the wall. We compared the spatial pattern of the map to the photo of the wall (Fig. 2) and to what we know about the condition of each particular ashlar to investigate whether there is any correlation between how the surface of the wall appears in visible wavelengths and what we know about the weathering of the surface and its temporal temperature behaviour. We speculate that the identified blue cluster separates the areas of the wall that are affected only by loss of material (i.e. alveolization and erosion) from other areas. The former are grouped in the blue cluster, while the latter are assigned to other clusters.

However, the large blue cluster includes ashlars of more than one surface type: it groups ashlars with strong alveolization (6 and 8) together with smoother surrounding ashlars (1, 2, 3, 4, 5, 7, 9 and 10). This means that in spite of their different stages of alveolization, they exhibit a similar temporal temperature trend and cannot be separated based only on their temporal behaviour. To try to separate ashlars 6 and 8 from the rest of this group, we later performed a second visual

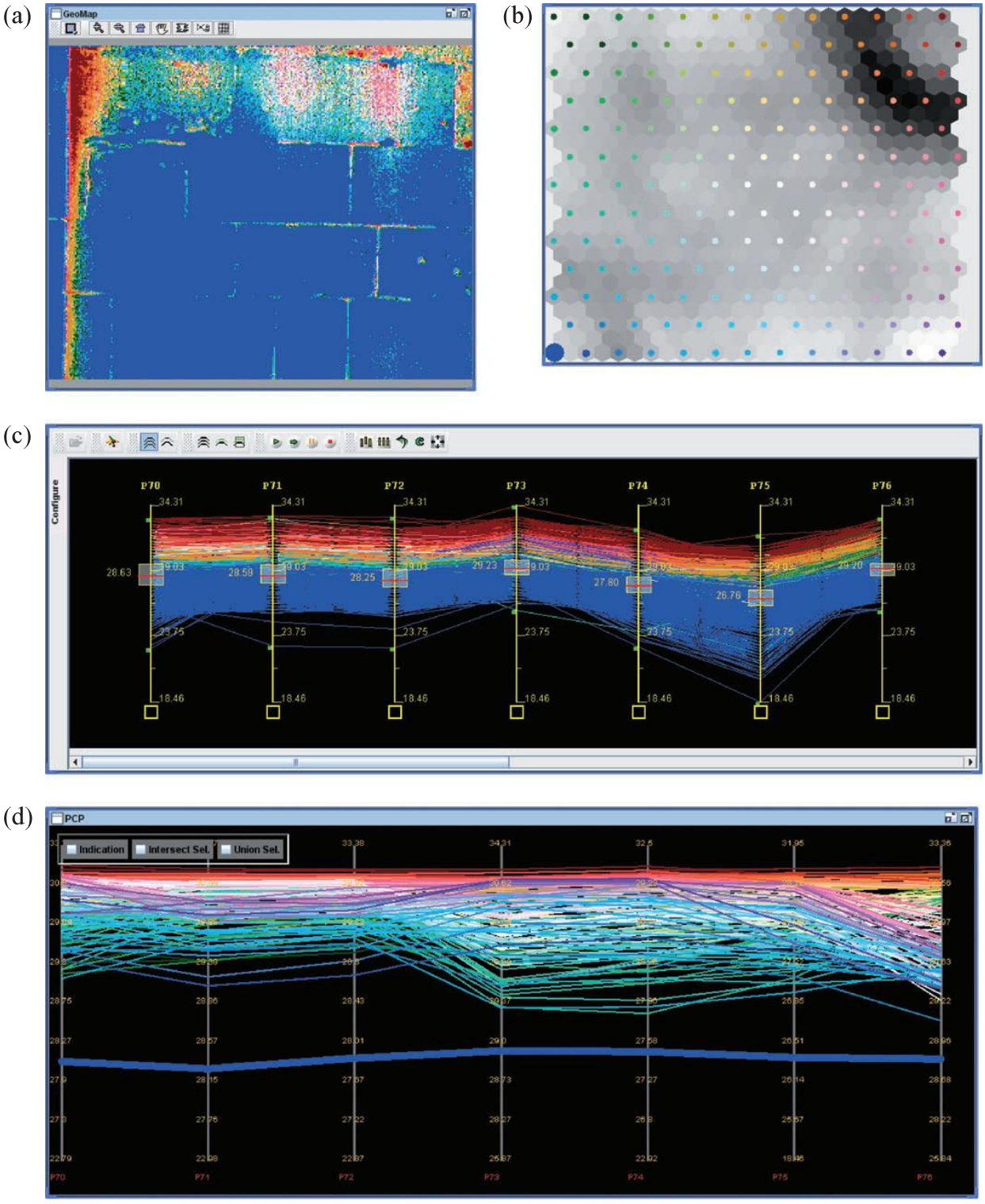


Figure 3 *Initial exploration of the dataset. Visualizations shown are (a) the map, (b) the SOM, (c) the temporal PCP and (d) the SOM PCP.*

exploration, by looking at the difference between the measured temperature of the wall and the external air temperature. This exploration is presented at the end of this section.

The temporal PCP in Figure 3(b) also shows a somewhat counter-intuitive temporal temperature trend, considering that the measurements were acquired in the evening, when the expected

behaviour would be that the wall gets cooler and cooler further along into the night. The temporal PCP (Fig. 3 (b)) shows that that the temperature range is 20–33°C at 21.00 (on the first axis, P70), that the wall proceeds to cool off towards 18–30°C at 23.30 (the second axis from the right, P75) and then warms up again to 25–32°C at 00.30 (the last axis on the right, P76). We know that from 22.00 onwards the external air temperature was relatively constant (Table 1), so no new heat was added to the wall. How, then do we explain the rise in wall temperature at 00.30? It is known in thermography that the variation of the temperature of the wall could be affected by presence of moisture in some parts of the wall, which could alter the expected temporal pattern of heat transfer (Maldague 2001). While it is beyond the scope of this paper to try to find out what is the particular reason for the unexpected increase in temperature in our case, this observation does show that visual exploration can identify unusual behaviour, which could be further analysed with other methods.

We continued our exploration by selecting clusters that are located far from each other in the SOM, i.e., the blue cluster and the red-orange cluster in the opposite corners of the SOM. The difference in their locations and the fact that there is an area of dark cells between the selected clusters means that they are very different from each other, which means that these clusters have very different temporal trends in temperature. The selection of these two clusters is shown in Figure 4.

There are two radically different trends present in SOM PCP of this selection (Fig. 4 (d)): the blue track has consistently low values of temperature and the red-orange track consistently high values. Neither blue nor red-orange clusters seem to correspond to any particular surface type from the visible light photo (Fig. 2). But we know that calcarenite, due to its porosity, is very sensitive to the presence of water, even when it is in its vapour state, and therefore also to the presence of condensation. We also know that water has a larger thermal inertia than stone, which means that when the external temperature decreases and the wall loses heat, the stone cools faster, while the water within the material remains warmer. The behaviour of the red-orange cluster is consistent with high thermal inertia and therefore points to the presence of water and helps us to understand where it is located in the wall. This hypothesis is also consistent with the particular position of the pixels from this cluster on the map (Fig. 4 (a))—they are located on the left border of the image, which shows the corner between two perpendicular walls (Fig. 2) and as such it is a place that is probably more difficult to dry out fully. The corner area probably has less interchange with the atmosphere and humidity should be present there to a larger extent than in other areas of the wall.

To explore the data further, we then performed the inverse selection in the SOM, i.e., we selected all other areas that were neither blue nor red-orange. Figure 5 shows this selection with pink, light blue and yellow-green clusters in the map and the SOM.

Investigating this selection in the map (Fig. 5 (a)) we see that the yellow-green pixels are closer to the parts of the wall where we have identified the possible presence of water, so this cluster is probably still related to humidity, although less than the red-orange cluster: it probably shows the border between the humid areas and the dry areas.

Looking at the map in Figure 5 (a), we noticed that ashlar 11 in the top left corner (Fig. 2) has a very peculiar behaviour, characterized by the simultaneous presence of many temporal clusters. As described in the previous section, there is a crust which is the remainder of a past protective treatment on this ashlar, which is consistent with our observation of many different behaviours across its surface. The behaviour of the surface of this ashlar cannot be homogeneous from the spatial point of view, because the depth of the remaining crust is not even and changes across the ashlar surface, which defines the temporal temperature behaviour. While the depth of the crust

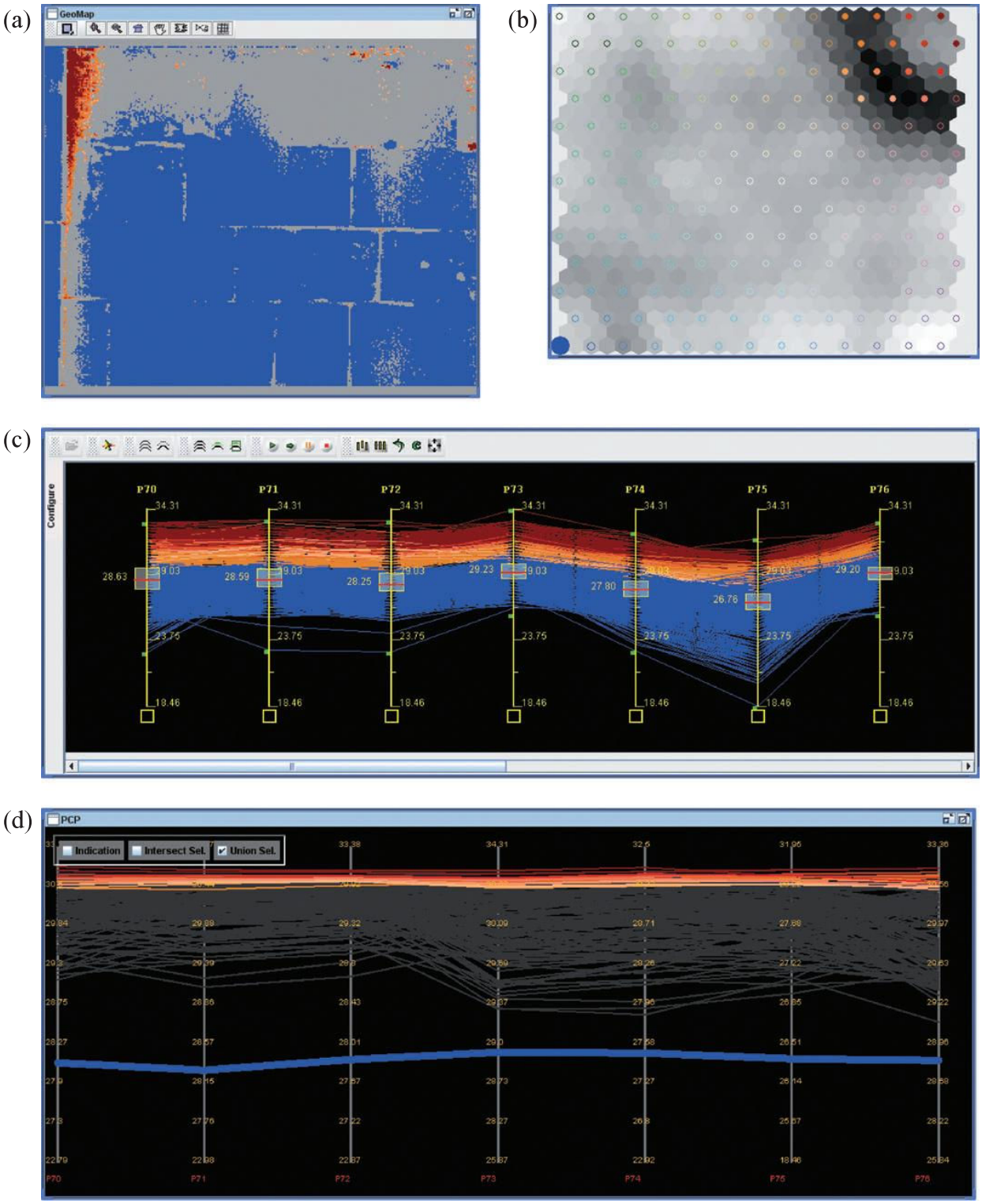


Figure 4 *The selection of the blue and red-orange SOM clusters shown in (a) the map, (b) the SOM, (c) the temporal PCP and (d) the SOM PCP.*

cannot be identified from the visual image (Fig. 2), this observation shows that visual exploration of thermographic data could help with identification of this particular phenomenon.

The pink cluster is spatially located in ashlar 12 (Figs 2 and 5). This pattern is an indicator that while something is likely to be happening in this part of the wall, this process is not visible from

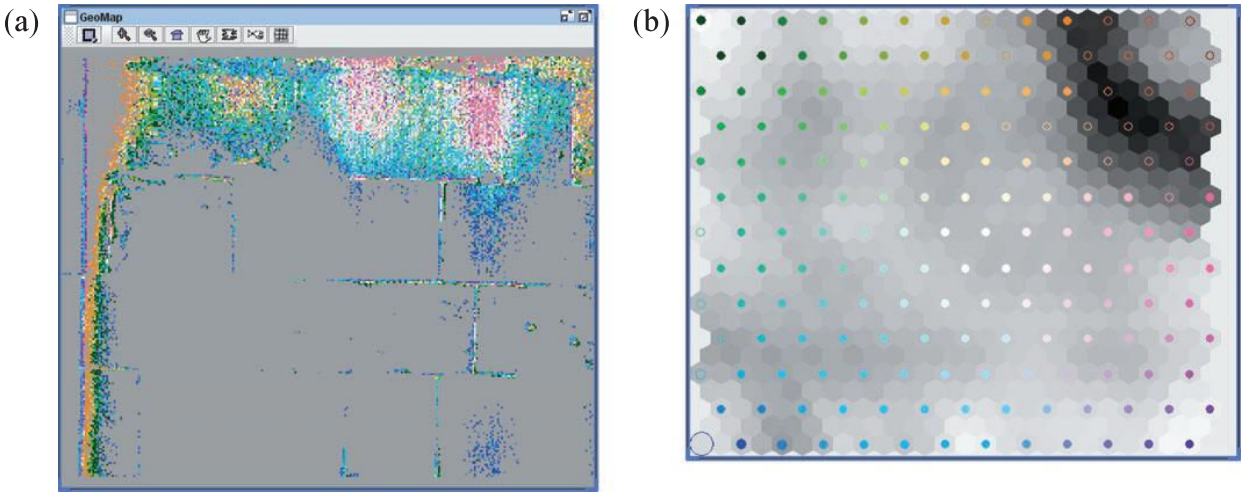


Figure 5 *The selection of the yellow-green, light-blue and pink SOM clusters shown in (a) the map and (b) the SOM.*

a macroscopic point of view since the surface of this ashlar appears relatively smooth (Fig. 2). While we do not have enough information to confirm what is happening in this part of the wall, we suspect that the identified behaviour could be related to some chemical or physical reactions in the stone, such as creation of particular salts. The pattern should therefore be studied further with other types of analysis (for example, chemical or physical analysis).

Another interesting pattern captured with this selection is the presence of loss of materials. In the location of ashlar 7 (Fig. 2), shown in the map in Fig. 5(a), we can clearly see both the loss of calcarenite in the two small holes in the centre of the ashlar as well as the disappearance of mortar between the ashlars in this general area.

To follow up the question that arose at the start of this analysis, i.e., how to separate the more eroded ashlars 6 and 8 from the rest in their cluster, we performed a second visual analysis, which was based on the difference between the measured temperature and the external air temperature. To do this, we calculated another SOM clustering on new attributes, which were defined as differences between the measured temperature of the wall in each pixel and the external air temperature ($T_{ext}$). These differences were calculated for each time, i.e., P70-$T_{ext}$ (at time P70), P71-$T_{ext}$ (at time P71), etc., until P76-$T_{ext}$ (at time P76). The SOM clustering in the following analysis is based on these differences and is a different clustering than before. Figure 6 shows the result. The temporal PCP (Fig. 6 (c)) is further extended with one additional axis labelled TEXTPOS, which is a Boolean attribute equal to 1 if the difference between the measured temperature and the external temperature was positive for all times, and 0 otherwise. This axis was added only to the temporal PCP; it was not included in the SOM clustering. The temporal PCP is also scaled differently than before. All axes, except the TEXTPOS, are scaled from –9.42 to 9.42°C, which is the absolute maximum value of the temperature difference across all times. This scaling was used to have 0 difference at the centre of all axes. The TEXTPOS axis is scaled from 0 to 1, as the Boolean attribute only has these two discrete values. As before, colours everywhere are defined by colours used in the SOM.

In contrast with the first exploration, the clustering based on temperature difference shows the separation between the areas with various levels of alveolization and identifies alveoli of different shapes and dimensions. The majority of the pixels are grouped into two lilac/violet clusters in the SOM (Fig. 6 (b)) and the tracks of these two clusters are consistently low in the SOM PCP (Fig. 6 (d)). These two lilac/violet clusters show a similar texture on the map (Fig. 6 (a)) as on the original photo (Fig. 2) and therefore indicate the level of alveolization.

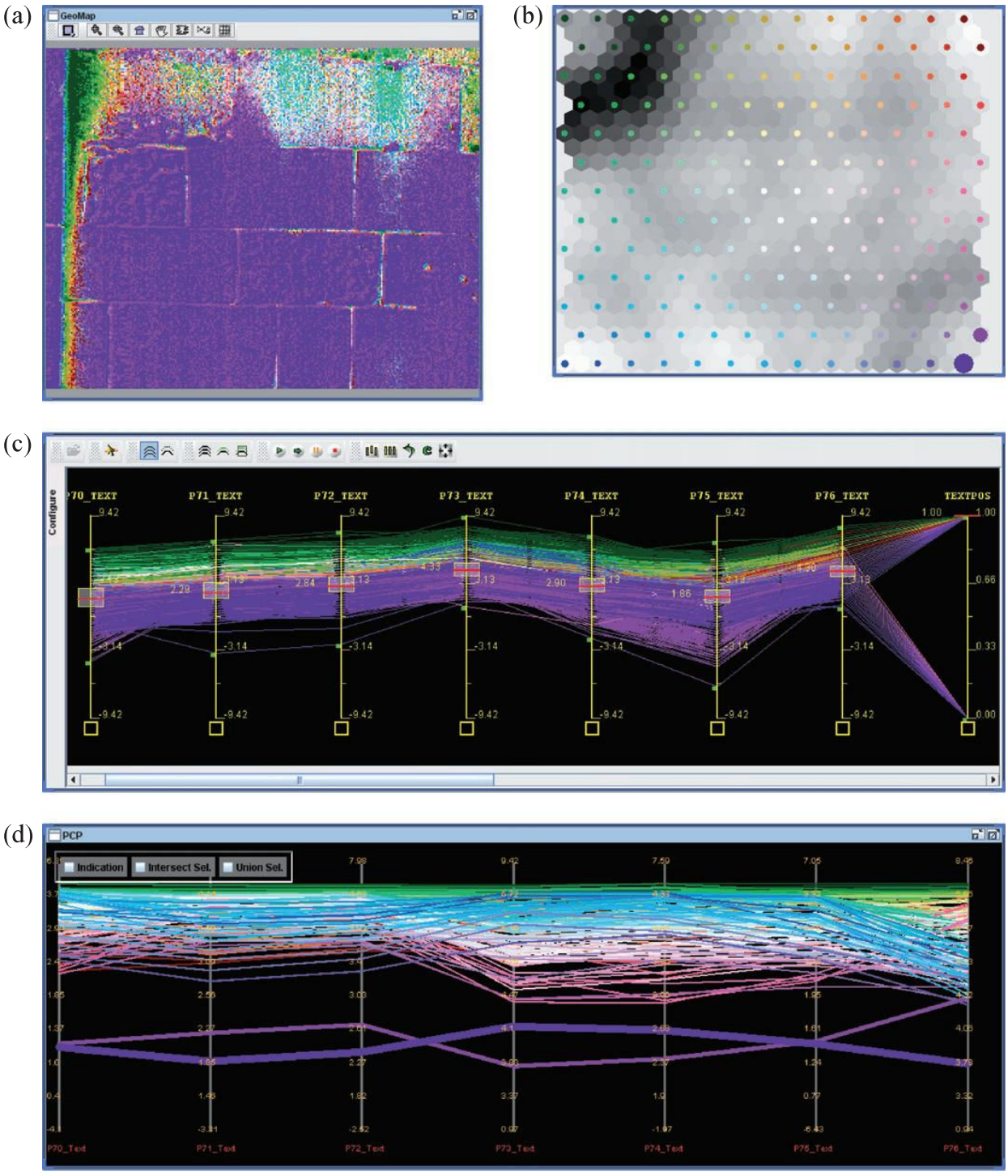


Figure 6 *Exploration based on the temperature difference shown in (a) the map, (b) the SOM, (c) the temporal PCP and (d) the SOM PCP. The temporal PCP has an additional axis with a Boolean variable TEXTPOS, which is equal to 1 if the temperature difference is larger than 0 at all times.*

The alveolization pattern can be further explored by selection on the TEXTPOS axis, which is shown in Figure 7. This selection shows only pixels where the TEXTPOS attribute has value 0, which corresponds to the areas where the difference between the wall temperature and the external air temperature was less than 0 at least once during the measurements, i.e., the areas of the wall which were cooler than the air in at least one measurement.

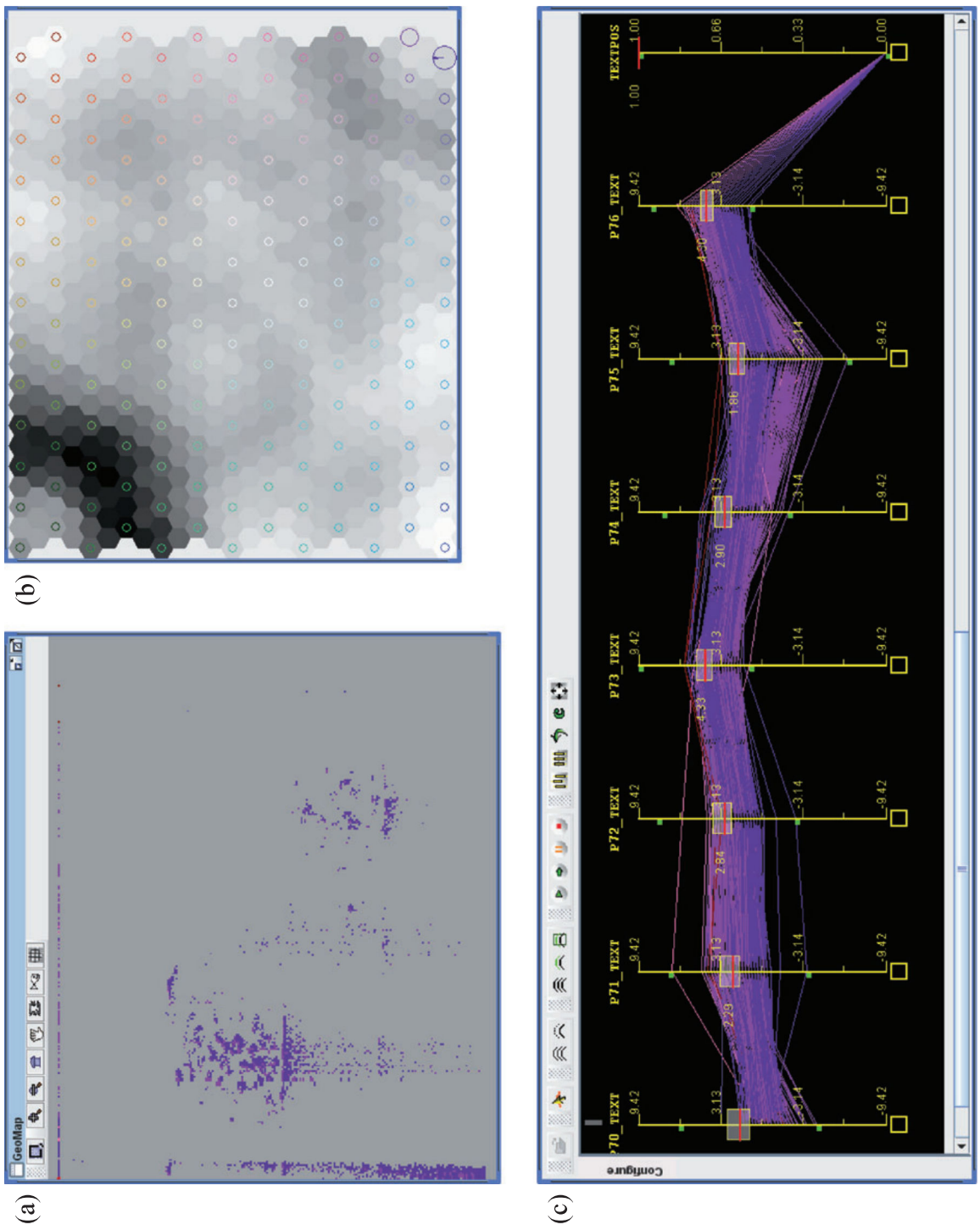


Figure 7 *The selection of areas with 0 value of the TEXTPOS attribute shown in (a) the map, (b) the SOM and (c) the temporal PCP. The selection was made in the temporal PCP.*

Table 2 *Summary of visually identified patterns*

| *Pattern no. (as in the Case Study section)* | *Description* | *Type of visually identified pattern* |
|---|---|---|
| 1–2–3–4 | Different levels of alveolization | Spatio-temporal clusters partly of temperature measurements and even more of temperature difference |
| 5 | Presence and depth of crust | Temporal clusters of temperature measurements |
| 6 | Presence of loss of material and behaviour of plaster between ashlars | Spatial clusters of temperature measurements |
| 7a | Presence of moisture in the corner area | Spatio-temporal clusters of temperature measurements and temperature difference |
| 7b | Ashlars 12 and 13: phenomenon not macroscopically visible and with an uncertain interpretation. Need to do more specific analysis | Presence of one zone of spatial spread of temperature and of one large spatio-temporal cluster of temperature measurements |

The spatial distribution of this selection on the map (Fig. 7 (a)) identifies the areas with the deepest and most widespread alveoli, in particular on ashlars 6 and 8 (Fig. 2). In these areas the heat exchange with the atmosphere is greatest due to convection, made possible by the large alveoli. This is reflected in negative values of temperature differences, as these areas grow cold faster than the rest of the stone where the surface is smoother.

The second clustering (based on temperature difference) also reconfirms phenomena that we have already observed in the first clustering (based on temperature). For example, the difference between the lilac/violet clusters and the green clusters, which are located opposite each other in the SOM in Figure 6 (b), points towards the same phenomenon—the presence of humidity in the corner areas—a phenomenon which was observed in the first clustering (compare with the selection of red-orange and blue clusters in Fig. 4).

## CONCLUSIONS AND DISCUSSION

In this paper we have demonstrated how visual analytics methodology can help with the interpretation of multi-temporal IRT data for cultural heritage restoration. In our experiment we were able to combine spatial and temporal analysis and identify patterns that point to different surface and material characteristics of the imaged wall by comparing the visually identified patterns to our knowledge about the wall. We could identify patterns that show different levels of alveolization and erosion of the surface, others that show the loss of material, and again others that show the level of humidity and the presence of water in the calcarenite. We also identified patterns that could not be explained by the analysis of the wall on a macroscopic scale, but which are potentially related to chemical and physical processes in the stone and which would have to be further confirmed with other types of analysis. The pattern and the related types of clusters found are summarized in Table 2 and can be compared with Figures 2, 3 and 6.

The experiment presented in this paper confirms that visual analytics could be used as an initial exploratory methodology for multi-temporal IRT data and facilitate its interpretation. Observations made can serve as a basis for hypotheses about the decay conditions of the wall and heat

processes in the wall. However, because this is, to our knowledge, the first attempt to explore multi-temporal IRT data in a visual environment, further analysis is necessary to confirm or reject some of the results found and the hypotheses made.

One known disadvantage of visual exploration is that the results cannot be easily quantified (Keim and Ward 2003) as the patterns that can be identified are only visual patterns, which cannot be evaluated numerically. This could be done with other spatial methodologies, for example spatial statistics or spatial analysis. The aim is to pass from the qualitative evaluation of visually identified patterns as presented in this work, to quantitative evaluation of the material decay. This would enable us to determine, for example, the total surface affected by a particular type and level of decay, which is necessary for restoration planning and policies.

Work presented here is only the first initial experiment on a limited case study, where the wall area under investigation was relatively small and consisted of one material only. We also only considered one type of weathering pattern, i.e., alveolization, to keep the data relatively simple. The reason for this was that the focus of the paper was to evaluate the new data exploration methodology rather than to make an in-depth analysis of the surface and structure of the wall. To achieve reliable results and be able to validate the identified patterns with weathering/material properties, the method would have to be tested further. Tests are required on both a global scale, where there are different weathering patterns present in one material, as well as on a single building scale, where the building consists of several different material types. In addition, other parameters would have to be considered both in thermographic data acquisition and in data analysis. These parameters include environmental factors (such as the aspect of the sun, wind speed and humidity) and material factors (such as geology of the materials in the building). While it is important that the new methodology undergoes rigorous testing before being applied to more complicated cases with any level of confidence, this first experiment shows that visual analytics exploration is a viable and promising methodology to facilitate interpretation of and acquire knowledge from multi-temporal IRT data for cultural heritage restoration purposes.

## ACKNOWLEDGEMENTS

The work of Urška Demšar and Martin Charlton was funded by a Research Professorship grant (03/RPI/1382) and a Strategic Research Cluster grant (07/SRC/I1168) both awarded to the National Centre of Geocomputation by Science Foundation Ireland under the National Development Plan. The authors gratefully acknowledge this support. Maria Danese wishes to thank the National Centre of Geocomputation, where the work was realized, for the kind and stimulating hospitality and Basilicata Region that financially supported her stay at NCG with the Moby Dick grant. The authors would also like to thank Daniela Sanseverino from the Institute for Archaeological and Monumental Heritage (CNR-IBAM) who was responsible for collection of the thermographic data used in this experiment.

## REFERENCES

Andriani, G. F., and Walsh, N., 2007, The effects of wetting and drying, and marine salt crystallization on calcarenite rocks used as building material in historic monuments, *Geological Society Special Publications*, London, **271**(1), 179–88.

Andrienko, G., Andrienko, N., Jankowski, P., Keim, D., Kraak, M.-J., MacEachren, A. M., and Wrobel, S., 2007, Visual analytics for spatial decision support: setting the research agenda, *International Journal of Geographic Information Science*, **8**, 839–57.

Avdelidis, N. P., and Moropoulou, A., 2003, Emissivity considerations in building thermography. *Energy and Buildings*, **35**, 663–7.

Avdelidis, N. P., and Moropoulou, A., 2004, Applications of infrared thermography for the investigation of historic structures. *Journal of Cultural Heritage*, **5**, 119–27.

Bação, F., Lobo, V., and Painho, M., 2005, The self-organizing map, the Geo-SOM and relevant variants for geosciences. *Computers & Geosciences*, **31**, 155–63.

Campbell, J. B., 1996, *Introduction to remote sensing*, 2nd edn, Taylor & Francis, London.

Demšar, U., 2007, Knowledge discovery in environmental sciences: visual and automatic data mining for radon problem in groundwater, *Transactions in GIS*, **11**(2), 255–81.

Demšar, U., Fotheringham, A. S., and Charlton, M., 2008a, Combining geovisual analytics with spatial statistics: the example of geographically weighted regression, *The Cartographic Journal*, **45**(3), 182–92.

Demšar, U., Fotheringham, A. S., and Charlton, M., 2008b, Exploring the spatio-temporal dynamics of geographical processes with geographically weighted regression and geovisual analytics, *Information Visualization*, **7**, 181–97.

Edsall, R. M., 2003, The parallel coordinate plot in action: design and use for geographic visualization, *Computational Statistics and Data Analysis*, **43**, 605–19.

Gahegan, M., Takatsuka, M., Wheeler, M., and Hardisty, F., 2002, Introducing Geo-VISTA Studio: an integrated suite of visualization and computational methods for exploration and knowledge construction in geography, *Computers, Environment and Urban Systems*, **26**, 267–92.

Geraldi, E., Gizzi, F. T., and Masini, N., 2004, Termografia All'infrarosso ed Archeologia Dell'architettura: Alcuni Esempi, in *Atti del 22° Convegno del Gruppo Nazionale di Geofisica delle Terra solida*, Sessione geofisica applicata di Beni Culturali, Rome, 18–20 November 2003.

Grinzato, E., Bison, P. G., and Marinetti, S., 2002, Monitoring of ancient buildings by the thermal method, *Journal of Cultural Heritage*, **3**, 21–9.

Grinzato, E., Vavilov, V., and Kauppinen, T., 1998, Quantitative infrared thermography in buildings, *Energy and Buildings*, **29**, 1–9.

Grinzato, E., Bison, P.G., Bressan, C., and Mazzoldi, A., 1997, The quantitative IR thermography for the diagnosis of frescoes, in *Proceedings of the 4th International Workshop on Advanced Infrared Technology and Applications*, 15–16 September, 345–66, Atti della Fondazione Giorgio Ronchi, Firenze.

Grinzato, E., Bison, P. G., Marinetti, S., and Vavilov, V., 1994, Non-destructive evaluation of delaminations in fresco plaster using transient infrared thermography, *Research in Nondestructive Evaluation*, **5**, 257–71.

Guo, D., 2003, Coordinating computational and visual approaches for interactive feature selection and multivariate clustering, *Information Visualization*, **2**, 232–46.

Guo, D., Gahegan, M., MacEachren, A. M., and Zhou, B., 2005, Multivariate analysis and geovisualization with an integrated geographic knowledge discovery approach, *Cartography and Geographic Information Science*, **32**(2), 113–32.

Hermosilla-Lara, S., Joubert, P. Y., Placko, D., Lepoutre, F., and Piriou, M., 2002, Enhancement of open-cracks detection using a principal component analysis/wavelet technique in photothermal non-destructive testing, in *Proceedings of QIRT'02 Conference*, 24–27 September, Dubrovnik, Croatia, 41–6, Office national d'études et de recherches aérospatiales, Châtillon, France.

Inselberg, A., 2002, Visualization and data mining of high-dimensional data, *Chemometrics and Intelligent Laboratory Systems*, **60**, 147–59.

Keim, D. A., and Ward, M., 2003, Visualization, in *Intelligent data analysis* (eds. M. Berthold and D. J. Hand), 2nd edn, 403–28, Springer, Berlin.

Kohonen, T., 1997, *Self-organizing maps*, 2nd edn, Springer, Berlin.

Koua, E. L., and Kraak, M.-J., 2004, Alternative visualization of large geospatial datasets, *The Cartographic Journal*, **41**, 217–28.

Ludwig, N., Redaelli, V., Rosina, E., and Augelli, F., 2004, Moisture detection in wood and plaster by IR thermography, *Infrared Physics & Technology*, **46**(1–2), 161–6.

Maldague, X. P. V., 2001, *Theory and practice of infrared technology for non-destructive testing*, John Wiley & Sons, New York.

Martinetti, S., Grinzato, E., Bison, P. G., Bozzi, E., and Cimenti, M., 2004, Statistical analysis of IR thermographic sequences by PCA, *Infrared Physics & Technology*, **46**, 85–91.

Meola, C., and Carlomagno, G. M., 2004, Recent advances in the use of infrared thermography, *Measurement Science and Technology*, **15**, R27–58.

National Visualization and Analytics Center (NVAC), 2005, *Illuminating the path: creating the R&D agenda for visual analytics*, available at http://nvac.pnl.gov/agenda.stm (last accessed 2 April 2008).

Rajic, N., 2002, Principal component thermography for flaw contrast enhancement and flaw depth characterisation in composite structures, *Composite Structures*, **58**, 521–8.

Rosina, E., and Grinzato, E., 2001, Infrared and thermal testing for conservation of historic buildings, *Materials Evaluation, ASNT Journal*, August, American Society for Nondestructive Testing, Columbus, OH.

Rosina, E., and Robison, E. C., 2002, Applying infrared thermography to historic wood-framed buildings in north America, *APT Bulletin*, **33**(4), 37–44.

Rosina, E., Ludwig, N., and Rosi, L., 1998, Optimal conditions to detect moisture in ancient buildings, study cases from northern Italy, in *Thermosense XX SPIE Proc. 3361*, Orlando, Society of Photo-Optical Instrumentation Engineers, Bellingham, WA.

Skupin, A., and Hagelman, R., 2005, Visualizing demographic trajectories with self-organizing maps, *Geoinformatica*, **9**(2), 159–79.

Vavilov, V. P., Kauppinen, T., and Grinzato, E., 1997, Thermal characterisation of defects in buildings envelopes using long square pulse and slow thermal wave techniques. *Research in Nondestructive Evaluation*, **9**, 181–200.

Vesanto, J., 1999, SOM-based data visualization methods, *Intelligent Data Analysis*, **3**, 111–26.